Scientific African 15 (2022) e01073

Contents lists available at ScienceDirect

Scientific African

journal homepage: www.elsevier.com/locate/sciaf

Effect of precursor concentration on corrosion resistance and microstructure of ZnO thin films using spray pyrolysis method

Victor Adewale Owoeye[a], Emmanuel Ajenifuja[b,c,d], Abiodun Eyitayo Adeoye[e], Ayodeji Olalekan Salau[f,*], Saheed Adekunle Adewinbi[g], Adedeji Tomide Akindadelo[8], David A. Pelemo[b], Abimbola Patricia I. Popoola[c]

[a] Department of Physical and Chemical Sciences, Elizade University, Ilara-Mokin, Nigeria
[b] Centre for Energy Research and Development, Obafemi Awolowo University, Ile Ife, Nigeria
[c] Department of Chemical, Metallurgical and Materials Engineering, Tshwane University of Technology, Pretoria, South Africa
[d] Centre for Energy and Electric Power, Tshwane University of Technology, Pretoria, South Africa
[e] Department of Physical Sciences, First Technical University, Ibadan, Nigeria
[f] Department of Electrical/ Electronics and Computer Engineering, Afe Babalola University, Ado-Ekiti, Nigeria
[g] Department of Physics, Osun State University, Osogbo, Osun State, Nigeria
[8] Department of Basic Sciences, Babcock University, Ilishan Remo, Nigeria

ARTICLE INFO

Article history:
Received 5 September 2021
Revised 1 November 2021
Accepted 15 December 2021

Editor DR B Gyampoh

Keywords:
Corrosion resistance
SPT
Microstrain
Molarity
Characterization
Thin films

ABSTRACT

This paper presents the preparation and characterization of ZnO at various molarities deposited on glass and 316L stainless steel (316L SS) substrates via spray pyrolysis technique (SPT) for multifunctional applications such as anti-corrosion of various types of steel in oil and gas companies , marine industry, and optoelectronic applications. Zinc acetate solution was employed as precursor. The X-ray diffractometry (XRD) result showed no significant effect on crystal size and microstrain when the molarity of ZnO increased from 0.1 M to 0.2 M, but with 0.3 M, the crystal size increased from 17.33 nm to 23.10 nm, while the microstrain of the film varied from 0.13 nm to 0.10 nm. The coated films' particles were observed to adhere suitably to the 316L SS substrate and were evenly distributed across the substrate surface. The results of the energy dispersive X-ray spectroscopy (EDX) and XRD affirm the presence of Zn and O in the deposited samples. The percentage of elements in the 316L SS are Fe = 70.10%, Ni = 10.10%, and Cr = 16.20% but on deposition of thin films. The signals of the Fe, Cr and Ni contents of the 316L SS were suppressed with increased ZnO concentration. The transmittance at the ultraviolet visible (UV-visible) region of (300 – 900 nm) showed that ZnO is highly transparent to visible light. The coated ZnO thin films improved the corrosion resistance of the 316L SS as seen from the electrochemical test result. Molarities were observed to increase with corrosion potential, which is related to corrosion resistance.The results show that the deposited ZnO coatings has a viable transparent oxide thin layer suitable for metal corrosion resistance.

* Corresponding author: Dr. Ayodeji Olalekan Salau, Department of Electrical/ Electronics and Computer Engineering, Afe Babalola University, Ado-Ekiti, Nigeria.
E-mail address: ayodejisalau98@gmail.com (A.O. Salau).

https://doi.org/10.1016/j.sciaf.2021.e01073

Introduction

Corrosion is the degradation of some properties of materials (metals and alloys) as a result of electrochemical reactions with their surroundings. The simplest type of corrosion is rusting which is formed because of the presence of hydrated ferric oxide on a metal surface. Electrochemical corrosion of metals and alloys is instigated by the transformation of electrons from metal surfaces by depolarizers [1].

316L stainless steel (316L SS) is used in many applications owing to its excellent properties such as high anti-corrosion potential, good thermal and electrical conductivity, and its excellent mechanical properties. The applicability of 316L SS in corrosion resistant applications such as naval, petrochemical, and pharmaceuticals is due to its ability to form passive film on its surface. The passive film is part of the layer of chromium oxy-hydroxide compound containing iron and water that are formed on the 316L SS interface by chromium oxide [1, 2]. The failure of 316L SS is however due to pitting corrosion of suphuric acid and chloride ions from hydrochloric acid [3].

The thin version of ZnO has a variety of applications in equipment and optoelectronic devices.For instance, it is used in direct conductors, gas sensors, sun-based cell windows [4–6]. ZnO is widely used in thin films development due to its abundance in nature and its non-toxicity [7, 8]. ZnO is one of the most widely considered transition metal oxides (TMOs) materials, with researchers all over the world considering its possible applications in a variety of new devices. ZnO is used in various applications due to its massive exciton binding energy (60 MeV) and appreciable room temperature band gap of 3.37 eV [9–11]. The applications of ZnO in recent times include optoelectronic device such as solar cell, gas sensor fabrication, photocatalytic degradation, photoanodes [12–15], and anti-corrosion protection of steels [16, 17]. A couple of works are available on the examination of ZnO applications in device creation and synthesis methods. . Regardless, because ZnO-based anti-corrosion, electrical, and optoelectronic devices are on the rise [18–20], the field of innovative devices made from this material has yet to be fully developed.

The research study of Babalola [14] recorded (002), (100), (101) and (110) X-ray diffractometry (XRD) peaks for 0.05 M ZnO without preferential orientation. ZnO film thickness examined by Rutherford backscattering spectroscopy (RBS) was observed to increase with concentration. The optical transmittance for all the categories of the films were observed to be estimated to 85% and observed to decrease with concentration; similar report had been previously reported by Chahmat et al. [21]. The work did not discuss the corrosion resistance of ZnO films. The I-V relationship of the study showed a linear relationship, while the resistivity was observed to increase with molarity. The XRD analysis of Jiang et al. [22] indicates that ZnO has a polycrystalline hexagonal structure with grain size found between 180 and 320 nm and film's transmittance was found close to 95% at a wavelength of 500 nm. The optical transmittance of ZnO in Kandasamy and Lourdusamy [23] was recorded as 70% in the visible region with direct bandgap values found in the range of 2.9 to 3.2 eV. Aydogu et al. [24] carried out a study on the deposition of pyrolyzed ZnO at a substrate temperature of 350°C. The films were observed to be polycrystalline and have energy bandgap of approximately 3.20 eV. The carrier electron density of ZnO was found to be 10^{23}–2×10^{-26} m^{-3}, while the electrical conductivity of the films was found to be 0.2–6×10^{-5} $\Omega^{-1}m^{-1}$ with an electron mobility in the range 10^{-40} cm^2/Vs.

The effect of nanoparticles ZnO films on 304L stainless steel using holmarc opto-mechatronics unit technique was carried in Muhamed et al. [16]. The results of the study show that the deposited films improved the corrosion resistance of the bare 304L steel bar before and after salt spray was applied. The study did not give any account of the effect of ZnO films on stainless steel in an acidic environment but give full account of its effect in saline environments. It was observed that the corrosion potential value of the bare 304L SS increased from −0.96 V to 0.41 V in an environment without salt spray, while the value was observed to change to 0.25 V in saline environment (after salt spray). The increase in the corrosion resistance of the steel was reported to be due to dispersal of the corrosive elements. A similar study was conducted by Hosseini et al. [25].

The corrosion potential of 316 L SS in acidic environment was reported to improve with increased Ni^{2+} in coated Ni-doped ZnO thin films using SPT in [17]. The corrosion resistance of mild steel in saline environment was reported to improve with coated composite NiO-ZnO thin films deposited by sol-gel method [26]. The anti-corrosion protection of coated TiO_2 thin films was reported to further improve with Al doping, corrosion resistance of stainless steel in acidic and saline media was improved with coated AlO_3-TiO_2 thin films deposited by atomic layer deposition reactor technique [27, 28]. The corrosion resistance of 316L SS was also reported to improve with coated ZrO_2, TiO_2-SiO_2 and Al_2O_3 thin films in basic and acidic media using sol-gel deposition method. However, it was evaluated that TiO_2-SiO_2 and Al_2O_3 thin films offered better anti-corrosion protection to 316L SS than ZrO_2 [29].

Cambon et al. [30] discussed the effect of Cerium concentration on corrosion resistance of X13VD martensitic stainless steel in saline and acidic environment using electrochemical impedance spectroscopy (EIS) technique. It was reported that Cerium concentration lesser or equal to 0.01 M gave the best corrosion resistance to the martensitic stainless steel. The corrosion resistance of Al-Mg alloys was examined to increase with scandium concentration due to formation of strong Sc_2O_3 passive film layer on the surface of the alloy [31]. The effect of neodymium ion (Nd^{3+}) addition as corrosion inhibitor of API X70 steel in saline environment was evaluated in [32], Nd^{3+} ions coating was observed to reduce corrosion rate of steel at a lower concentration of 0.001 M. The inhibition efficiency was observed to be slightly affected at higher concentrations. The formation of a protective layer of oxides/hydroxides on the metal surface was initiated by $+e$ adsorption of the Nd^{3+} ions.

The ZnO in this study was prepared using one of the bottom-up methods of nanostructuring material which is quite different from top-down approaches due to the uniqueness identified in their properties [13, 17, 33]. Thin film has been

defined as the coating of material usually less than one micrometer in thickness compared to thick film whose thickness is greater than one micrometer. Even the human hair, which is thicker than thin film is supported by scalp. Hence, thin films because of their thinness, are fragile and not self-supporting. They are usually supported by carriers called substrates. A substrate is usually many times thicker than the film on it [34].

In recent times, the various substrates to which thin films can be deposited include steels, glass slides, indium tin oxide (ITO) glass and others. The demand for new things and devices in the electrical, optical, and other industries is propelling thin film innovation forward at a rapid pace. The quick progress in nanotechnology would not have been conceivable without the advancement of new sorts of thin films deposition processes, improved film attributes, and film characteristics. There are two major techniques for film deposition, namely: chemical vapor deposition (CVD) and physical vapor deposition (PVD) processes. Solgel, electrodeposition, chemical spray pyrolysis etc. are few examples of CVD. Laser ablation, sputtering, evaporation, molecular beam epitaxy are the examples of PVD process [35–38]. Spray pyrolysis technique (SPT) is employed in this study because of its enormous benefits over other deposition techniques [39–42]. Research studies show that deposition conditions such as molarity/concentration, deposition temperature, deposition volume and duration can affect the properties of the films produced [4].

The loss of materials to corrosion process has resulted to a serious problem in many industries. Most industries around the world are often faced with the challenges of how to overcome the loss they usually account for due to the huge amount of money being spent on the maintenance of damaged facilities caused by electrochemical degradation. Stainless steel is used in most of these industries for various applications because it offers a wide range of alloys and qualities that provide enormous benefits to the vast range of processes used in modern industries. However, researchers must find the easiest ways by which corrosion resistance of stainless steel can further be improved because many corrosive compounds i.e., sulphuric acids, hydrochloric acid, polythionic acids, ammonium chloride which are formed during its applications at a wide range of operating temperatures affect the corrosion resistance of stainless steel. This present study investigates effect of concentration on corrosion resistance of coated ZnO thin films on stainless steel in acidic media. The choice of ZnO is chosen as surface protection of 316L stainless steel because of its various exciting properties as discussed in this study. This study provides additional information on the coating methods for stainless steel as applicable in the various manufacturing industries.

Methodology

Materials

Two substrates were used in this research study. 316L SS substrate was used to examine the corrosion resistance and microstructure of ZnO thin films. The choice of soda lime glass substrate was later considered to evaluate the level of transmittance of ZnO because it was observed from scanning electron microscopy (SEM) that the grains in 316L SS were also revealed after ZnO deposition. The nominal composition of the 316L SS is presented in section 3 of this study. The 316L SS used was a flat material with 1.6 mm stiffness which was machined to a sample dimension of 28.5 mm by 12.4 mm for all the tests carried out. The source precursor employed was pure zinc acetate soluble in distilled water. Zinc acetate was chosen over other precursors because of its numerous benefits as pointed out in [13].

ZnO thin films preparation

Different molarities of ZnO were prepared by spraying 20 ml of liquid zinc acetate precursors on pre-heated ultrasonically cleaned 316L stainless steel and glass substrates at a temperature 350 °C using a low power consuming and easy to operate SPT. The precursors were prepared at different molarities (0.1 M-0.3 M) in distilled water to vary the metallic constituents of the films. 0.1 M of liquid zinc acetate precursor was obtained by mixing 0.66 g of zinc acetate in 30 ml of distilled water. This quantity was obtained from Eqs. (1a) to (1f) and then measured using a weighing balance before dissolving it in 30 ml of distilled water.

The parameters needed for the 0.1 M of liquid zinc acetate precursor are:

219.50 g/mol = molar mass of zinc acetate ($Zn(CH_3COO)_2{\bullet}2H_2O$),
Volume of distilled water (V_f) = 30 ml
Molarity = 0.1 M
Volume (L) = 10^{-3} m^3
1 $L = 10^{-3}$ m^3

Recall,

$$Molar\ concentration = \frac{Amount\ (mol)}{Volume\ (L)} \tag{1a}$$

$$Amount\ (mol) = \frac{mass\ (g)}{molar\ mass\ \ ((g/\mathrm{mol})} \tag{1b}$$

Table 1
Sample codes and molarity of deposited zinc acetate precursor solutions.

Sample Name	zinc acetate precursor solutions
Z0	316L Stainless steel (Control)
Z1	0.1 M zinc acetate precursor (20 ml)
Z2	0.2 M zinc acetate precursor (20 ml)
Z3	0.3 M zinc acetate precursor (20 ml)

Substituting (1b) for Amount (mol) in (1a)

$$Molar\ concentration = \frac{Mass}{Molar\ mass\ \times Volume} \tag{1c}$$

$$mass = molar\ concentration \times molar\ mass\ \times Volume \tag{1d}$$

$$mass = molarity \times \upsilon_f \times molar\ mass \times 10^{-3} \tag{1e}$$

Where volume (L) = 10^{-3} m^3

$$mass = 0.1 \times 30 \times 219.5 \times 10^{-3} = 0.66\ g \tag{1f}$$

From (1f) 0.66 g of zinc acetate was liquefied in 30 ml of distilled water to obtain 0.1 M of liquid zinc acetate precursor, the same procedure was used to obtain 0.2 M and 0.3 M. Table 1 illustrates sample codes and molarity of deposited zinc acetate precursor solutions.

The liquid precursor solutions were stirred briskly and allowed to dissolve for few seconds before spraying on the substrates. All deposition parameters were optimized to achieve quality films [13]. Eq. (2) gives the chemical reaction of how ZnO was obtained from spray pyrolyzed liquid zinc acetate precursor at 350 °C.

$$Zn(CH_3COO)_2.2H_20_{(aq)} \xrightarrow{\Delta} Zn0_{(l)} + 2CO_{2_{(g)}} + 2CH_{4_{(g)}} + H_2O_{(g)} \tag{2}$$

Characterization

The morphology of the samples was examined using scanning electron microscopy (SEM); the samples' elemental composition was evaluated using JOEL JSM-7600F FE-SEM energy dispersive X-ray spectroscopy (EDX). The microstructure of the 316L SS and the deposited films was analyzed using PW1710 Philips XRD incorporated with Cu radiation at potential of 40 kV and current of 40 mA. The diffractometry data from the XRD was analyzed by PANalyticalX'Pert High Score software. The film's optical transmittance on soda lime glass was determined using ultraviolet visible spectrophotometer.

Corrosion resistance measurement

The corrosion potential of both 316L SS and the coated samples was evaluated in 0.1 M of H_2SO_4 solution with an exposed surface area of 20 mm^2. To ensure the surface area to be tested for corrosion was differentiated from the other surface , the other surfaces of the samples were covered with epoxy to prevent corrosion attack on both surfaces. Three electrodes; the samples (working electrode), silver chloride (reference electrode), and platinum (counter electrode) were used for the corrosion experiment. Autolab potentiostat galvanostat (PGSTAT) setup was used for the corrosion experiment, while the corrosion current was obtained using the galvanostat as potentiostat measured the corrosion potential of the samples. According to [17, 43], corrosion potential is proportional to corrosion resistance, the corrosion potential of the samples was obtained from the plot of corrosion potential versus corrosion current. The electrochemical test arrangement given in Owoeye et al. [17] was also used in this study.

Results

Microstructures of the samples

The crystal structures of the uncoated and coated samples were examined by XRD. Thin films deposited were observed to have crystalline morphology as confirmed by comparing the XRD pattern of Z0 in Fig. 1(a) to Figs. 1(b)−1(d). The films were made of single phase ZnO having quite a few diffraction peaks. The observed XRD diffraction peaks (002) at angle 2θ using Reference code (01–079–0208) corresponds to ZnO having hexagonal wurtzite structure and a preferential c-axis orientation [4, 5, 22, 17, 24].

The XRD spectrum of Z0 is shown in Fig. 1(a). There are three observable diffraction peaks in the spectrum with the prominent peak found at position of $2\theta = 74.43°$. The prominent peak has a total height of 3241.56 cts and 0.6 full width at

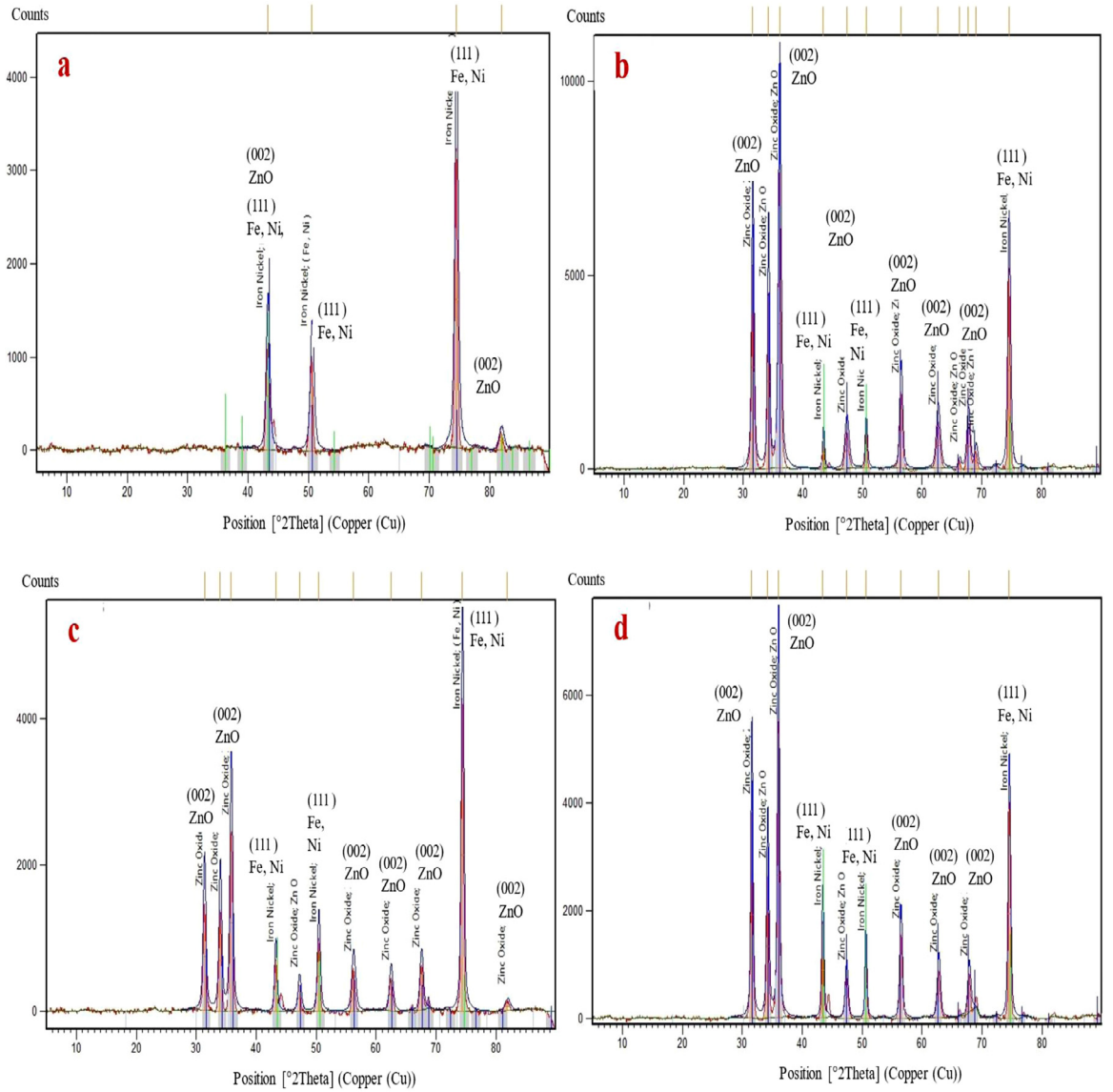

Fig. 1. XRD patterns of the structures (a) Z0 (b) Z1 (c) Z2 (d) Z3.

half maximum (FWHM). However, from the Figure, it was observed that Z0 is highly crystalline with the peak showing the presence of Fe and Ni in the stainless steel. The peaks at angle 2θ correspond to Ni and Fe with reference code (00–023–0297) face centered cubic (fcc) crystal structure.

Fig. 1(b) shows the XRD spectrum of Z1. Several peaks were identified in the pattern showing that the film is more crystalline when compared to the uncoated steel presented in Fig. 1(a). There are many observable diffraction peaks in the spectrum with the prominent peak found at position of $2\theta = 36.11°$. The prominent peak has a total height of 7615.68 cts and 0.54 FWHM. The XRD spectrum of coated Z2 is shown in Fig. 1(c). Several peaks were also observed in the pattern with the prominent peak found at position of $2\theta = 74.34°$. The prominent peak has a total height of 4364.64 cts and 0.45 FWHM, and seems to originate from 316L SS substrate. The prominent diffraction peak corresponding to the coated film is found at $2\theta = 35.8°$ with total height 489.84 cts and 0.54 FWHM. The XRD spectrum of coated Z3 is shown in Fig. 1(d). Several observable peaks were also identified in the pattern with the prominent peak found at the position of $2\theta = 36.0°$. The prominent peak has a total height of 5378.97 cts and 0.40 FWHM.

In Table 2, the summary of the influence of molarities on ZnO microstructure is presented. It was observed that with increase in molarity, the average crystal size increases. The average crystal size was obtained using Eq. (3). It was observed that Z1 has the same value with Z2, and this value increases significantly from 17.33 nm of Z1 to 23.10 nm of Z3. The position 2θ was also observed to vary with molarities. The prominent peak in Z1 spectrum was observed at $2\theta = 36.11°$,

Table 2
Concentration effect on ZnO structure.

Samples	Pos. ($2\theta°$)	d-spacing (Å)	FWHM	Crystal Size (nm)	Microstrain
Z1	36.11	2.49	0.54	17.33	0.13
Z2	35.83	2.51	0.54	17.33	0.13
Z3	36.01	2.49	0.40	23.10	0.10

the value reduced to 35.83° and 36.01° of Z2 and Z3, respectively. The effect of molarities on the microstrain of ZnO is also presented in Table 2 using Eq. (4). The microstrain was calculated to be 0.13, 0.13 and 0.10 for Z1, Z2 and Z3, respectively. It was observed that microstrain of ZnO thin films decreases with molarity. The height and width of the peaks are also observed to change with molarity, it was observed that the total height of coated Z1 corresponds to 7615.68 cts, the value changes to 22,489.84 cts and 5378.97 cts of Z2 and Z3, respectively. The observable change in the structure of the films was due to the increase in the mass of the precursor with increase in the molarity. The changes may also result from the heat treatment of the stainless steel because they were pre-heated before deposition.

The conclusion from the XRD analysis, show that no significant effect on crystal size and microstrain was observed when the molarity of ZnO increased from Z1 to Z2, but with Z3, the crystal size increased greatly from 17.33 nm of Z1 and Z2 to 23.10 nm of Z3. The microstrain was observed to reduce from 0.13 nm of Z1 and Z2 to 0.10 nm of Z3. This means that the crystals tend to agglomerate to form single crystals with reduced deformation which likely cause the strain to be lowered. One would expect that the microstrain would have been lower for the small crystals and lower at 0.1 M when the crystals are of small sizes and can fit very well together, but in this case, there seem to be more of defect than when large crystals sizes were obtained. With many fine grains and small crystal sizes, the films formed tend to be more of polycrystalline which may be the cause of higher microstrain.

The crystallite size in this study was determined from Debye-Scherrer equation given by Eq. (3) [44].

$$D = \frac{K\lambda}{\beta COS\alpha} \tag{3}$$

D = crystallite size
K = Debye constant = 0.90
λ = wavelength of the X-ray with value equal to 0.15406 nm
α = Bragg angle
β = FWHM is determined for each angle [45].

The microstrain (ε_s) often refers to overall change in the lattice parameters. Because of change in composition, pressure and temperature are calculated using Eq. (4)

$$\varepsilon_s = \frac{\beta \cos\theta}{4} \tag{4}$$

where θ is the diffraction angle for a particular plane.

Morphological properties of the samples

The micrograph of Z0 is shown in Fig. 2(a), while Figs. 2(b-d) illustrate the SEM micrographs of coated Z1, Z2 and Z3, respectively. The SEM micrograph displayed in Fig. 2(a) shows that 316L SS has many grains in its structure. The grains were also revealed after they were coated with various molarities of ZnO as shown in Figs. 2(b-d). This was due to the substitutional diffusion of ZnO structure as the films penetrated the 316L substrate. This may also be due to the film's transmittance and thickness. However, the grains in the 316L steel were observed to be slightly covered when coated with ZnO, while the colors of the coated ZnO films were observed to change with molarity. ZnO films improved the surface morphology of 316L SS and there is an improvement in the surface with increase in the molarity of the samples. The coated films were observed to adhere suitably to the 316L stainless steel substrates with evidence of good growth on the substrate surface [46]. The tendency for heavy and localized grains to appear on the surface is a result of ZnO degeneracy. Nucleation site number was observed to increase by increasing the concentration of ZnO [47, 48].

Samples' elemental composition

In Fig. 3(a-d), the EDX shows the peaks of the compositions of some of the selected areas of the SEM images displayed in Fig. 2(a-d). The images confirm the existence of deposited Zn and O in the films. The XRD spectra in Figs. 1(b-d) also validate the EDX result. The other elements shown in the EDX images are from the 316L SS substrate. The main elements of the 316L SS are Fe = 70.10%, Cr = 16.20% and Ni = 10.10%. The elements present in Z1 are in the proportion of Fe = 69.20%, Cr = 16.20%, Ni = 9.60%, O = 1.90% and Zn = 1.60%. The elements present in Z2 are in the proportion of Fe = 62.70%, Cr = 14.80%, Ni = 9.10%, O = 4.8% and Zn = 7.1% while Z3 are in the proportion of Fe = 57.10%, Cr = 13.90%, Ni = 7.60%, O = 6.00% and Zn = 11.60%. Fig. 3(a-d) and Table 3 summarize the effect of concentration (molarity) on the elemental

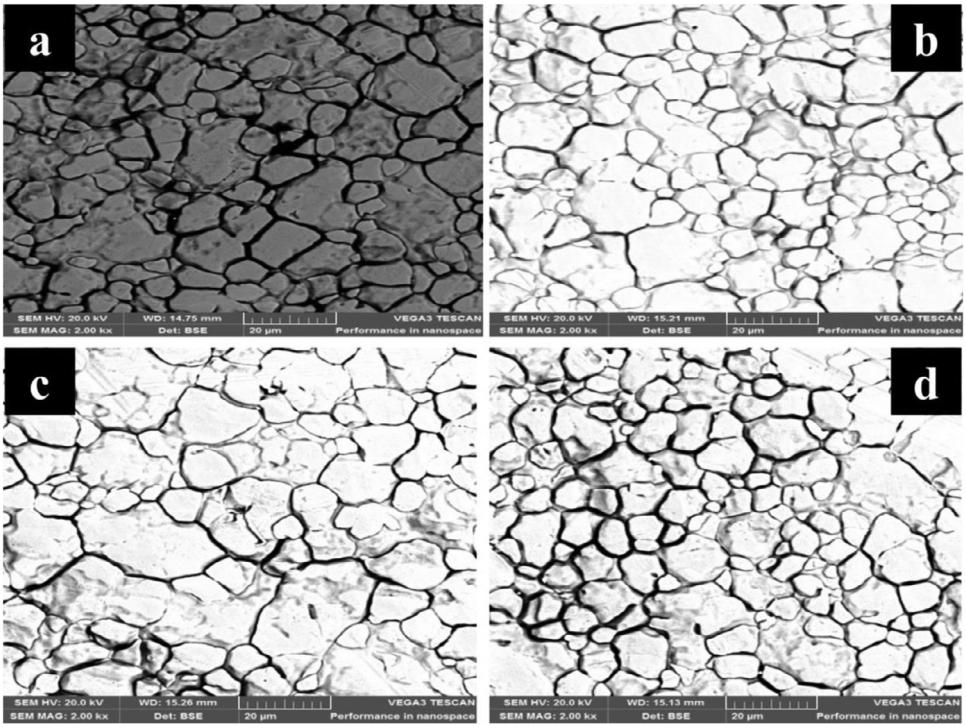

Fig. 2. SEM micrograph of (a) Z0 (b) Z1 (c) Z2 and (d) Z3.

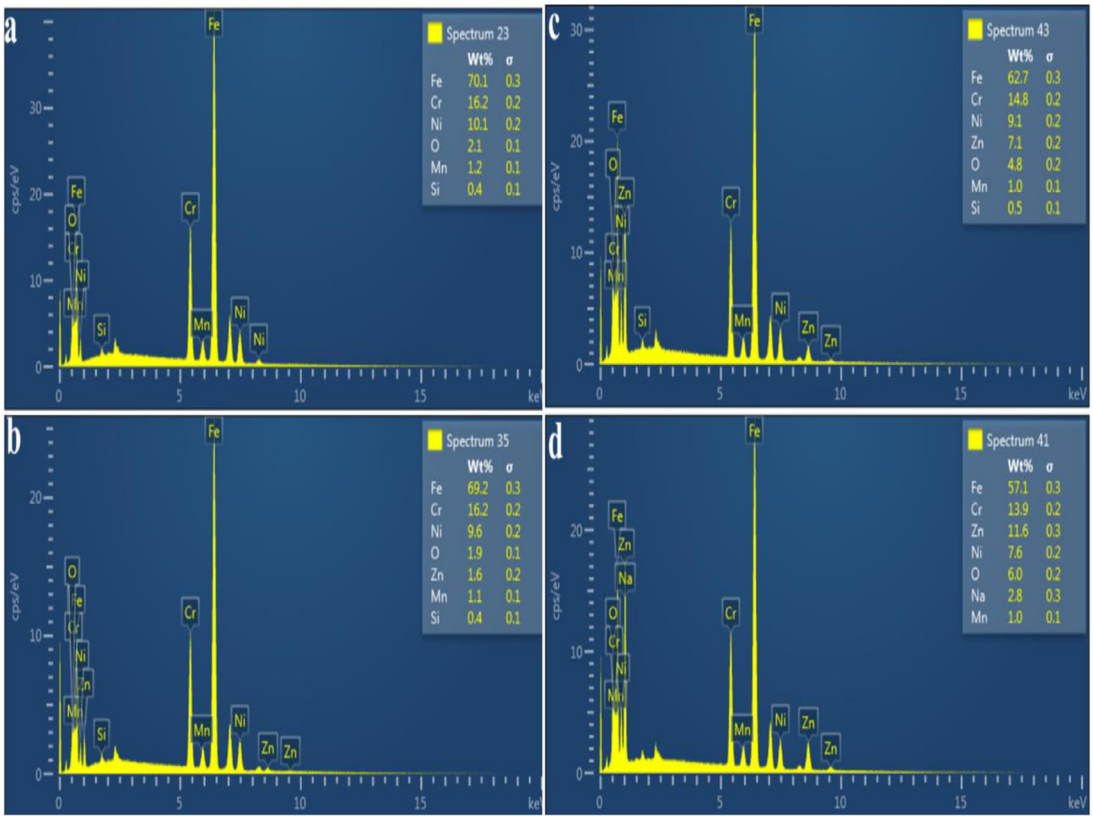

Fig. 3. EDX of (a) Z0 (b) Z1 (c) Z2 (d) Z3.

Table 3
Effect of Molarity on the Elemental Composition of ZnO Thin Films.

Samples	Fe (%))	Cr (%)	Zn (%)	Ni (%)	O (%)	Others (%)
Z0	70.10	16.20	–	10.10	2.10	1.50
Z1	69.20	16.20	1.60	9.60	1.90	1.50
Z2	62.70	14.80	7.10	9.10	4.80	1.50
Z3	57.10	13.90	11.60	7.60	6.00	3.80

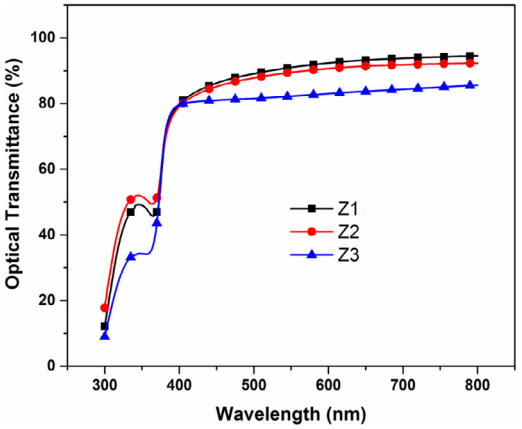

Fig. 4. Transmittance of samples Z1, Z2, and Z3.

Table 4
Samples (%) transmittance.

Sample	Peak Transmittance (%)
Z1	94.00
Z2	92.00
Z3	86.00

composition of ZnO films deposited on 316L SS. The key elements in the 316L stainless steel are Fe = 70.10%, Cr = 16.20% and Ni = 10.10% but for the deposition of thin films, the signals of the Fe, Cr and Ni contents of the stainless steel were suppressed with increase in the concentration of coated ZnO films. The compositions as determined for Zn and O increase consistently with molarity. This is an indication that zinc and oxygen were closely bonded.

Concentration effect of ZnO optical transmittance

The optical transmittance of the deposited samples on soda lime glass in the UV-visible spectrum (300 – 900 nm) is shown in Fig. 4. The films exhibit high transparency (80–95%) in the visible range. This agrees with earlier results obtained using doped ZnO and undoped ZnO thin films [13, 22, 49]. It is also expected that as the molarity increases, the film thickness will increase; the relationship between ZnO film thickness and molarity was reported in [14]. The study reported that ZnO film thickness increases with increased molarity. Therefore, film thickness reduces the optical transparency because of their inverse proportionality. The transmittance of the films was observed to decrease with increased molarity as expected because the crystal will become more densely populated with increased concentration (Table 4). Similar results were reported in [14, 21]. Indications from the transmittance plots show that the samples generally exhibit humps at a region surrounding $\lambda \sim 330$ nm situated at the ultraviolet (UV) region of the spectra. This property was also found to be dependent on the molarity of the film's precursor. This observable feature indicates the influence of oxygen vacancy ascribed to the intrinsic bang gap absorption attributable to some mesoporous metal oxide nanostructure which varies with our films' thicknesses. This result also exemplifies the role of these materials as recombination inhibitors and photocatalytic agents in thin film based photonic devices [50–52].

The samples' electrochemical properties

The Figs. 5(a-e) are known as polarization curves and were obtained using autolab Potentiostat Galvanostat (PGSTAT) technique. The potentiostat measures the potential of the counter electrode (CE) against the working electrode (WE). The values obtained from this device were plotted against the current flow between the WE and CE as measured using the Galvanostat. In Eq. (5), the corrosion resistance is said to be proportional to polarization potential (corrosion potential) as

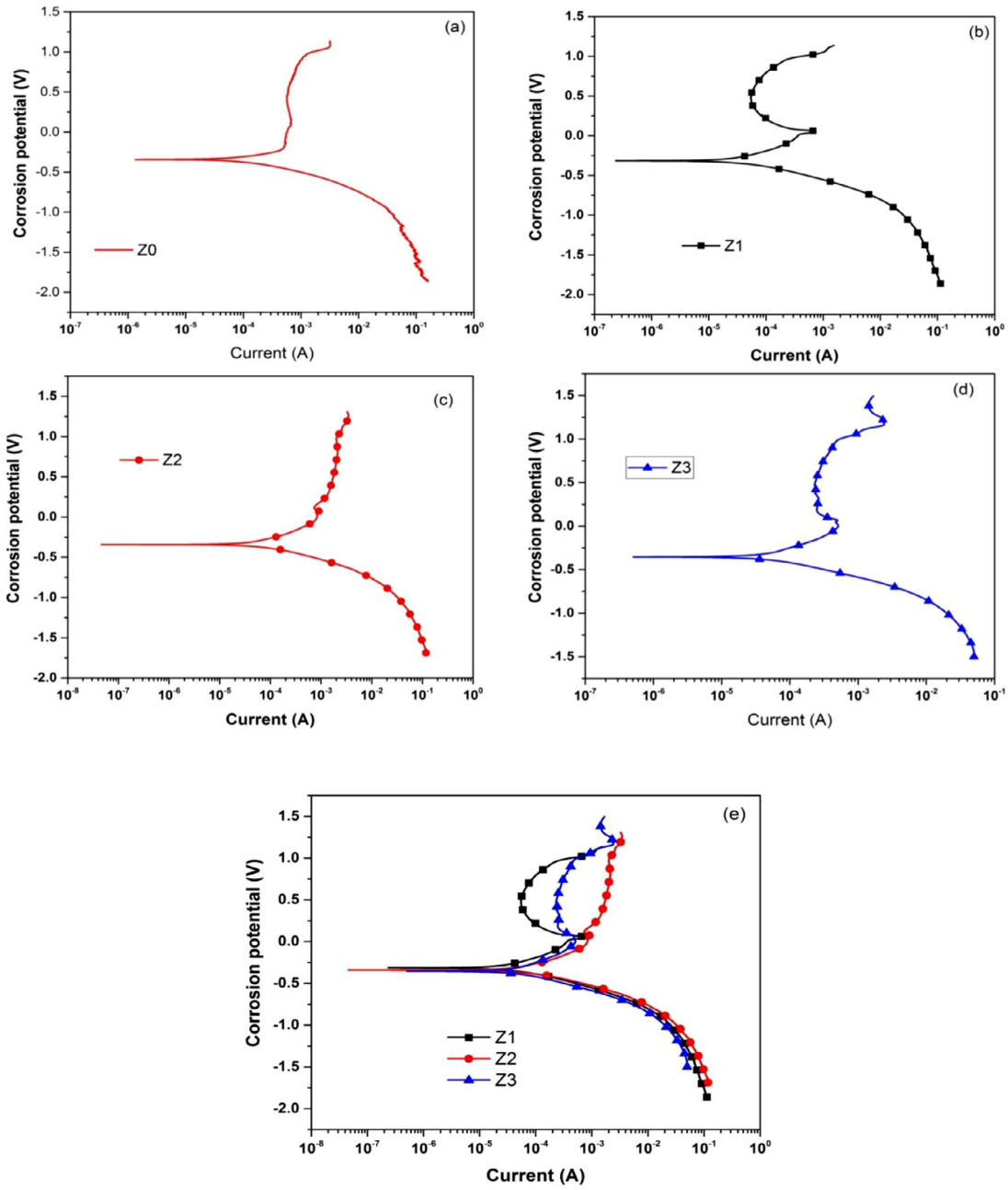

Fig. 5. (a-e) The samples' polarization curves.

stated in Tang [43]. Table 5 gives the summary of the values of the corrosion potential. From the results presented in the table, the coated films enhanced the corrosion potential as well as corrosion resistance of 316L SS. The corrosion potential was observed to increase with molarities with coated Z3 having the highest value of corrosion potential as compared to other coated samples in the curves. The increase in the corrosion potential of 316L SS as the molarity increases was due to increase in Zn content of the coated films as shown in Table 5. Zinc coating is one of the best corrosion protection methods used in steel coating because it offers cathodic protection to steel due to its ability to prevent moisture and oxygen from directly affecting the surface of the steel [17].

The rise in the corrosion potential of the 316L SS when coated with ZnO films may also be due to the addition of Zn into the surface of the steel because zinc has a lower reduction potential than iron which happens to be the major component of the 316L SS as shown in Table 3. The high reduction potential of zinc makes it a more active metal at the surface of steel, which oxidizes before iron even if its coating is deteriorated. The improvement in the corrosion resistance of the 316L

Table 5
Corrosion potential (CP) of the samples.

Samples	CP (V)
Z0	1.20
Z1	1.25
Z2	1.35
Z3	1.50

SS may have also resulted from the protective layers of the ZnO thin films on the material's surface. From Table 3, it is observed that the signals of Fe, Cr, and Ni play a critical role in the resistance of steel to corrosion . The coated ZnO thin films also form additional passive film layers on 316L SS surface because corrosion resistance of stainless steel in general is accredited to diffusion of the corrosive passive films into the parent material [53]. Studies have shown that the corrosion properties of steel are characterized by the formation of Cr passive film layers on steel, formation of chromium passive film layers on steel which result in improvement of the corrosion resistance of steel [53, 54].

The curves in Fig. 5(a-e), were observed to shift to higher corrosion potentials with increase in molarity of coated ZnO thin films. The positive shift in the corrosion potential as molarity of ZnO increases is also an indication of increase in corrosion resistance [19]. This signifies that the corrosion protection of the 316L SS improves with molarity of coated ZnO. The shift to a higher positive corrosion potential is a function of the corrosion protection [25], as the working electrode was observed to have shifted into the passive region. It was noticed that the coated ZnO films improved the corrosion performance of the 316L stainless steel. Passivation has been reported to reduce the anodic reaction involved in the corrosion process [17, 53]. The resistance of stainless steel to corrosion is often estimated by their passivation characteristics, elemental composition such as Fe, Cr and Ni, heat treatment and the corrosive medium [54–56].

$$R_p = \frac{\partial E_p}{\partial I_p} = \frac{\Delta E_p}{I_p} \tag{5}$$

$$\mathbf{I_p \rightarrow 0, \quad as\ E_p \rightarrow\ E_{corr}}$$

where R_p = polarization resistance = corrosion resistance

E_p = polarization potential = corrosion potential and I_{corr} = corrosion current.

Conclusion

The influence of molarity on the structural properties and corrosion resistance of ZnO films coated using SPT on 316L SS was investigated in this study. Different molarities of zinc oxides were prepared from pure zinc acetate precursor solution. The EDX images confirmed the deposition of Zn and O in the films, and the XRD pattern validated the EDX result. The XRD result showed that both the uncoated 316L SS and coated films have crystalline morphology and all the films formed a single ZnO phase. The crystal size increased from 17.33 nm to 23.10 nm based on the level of molarity and in the same vein, the microstrain was observed to reduce from 0.13 nm to 0.10 nm. The UV result showed that films transmittance decreased with increased molarity. The SEM micrograph showed that 316L SS has many grains in its structure, and the signals of the Fe, Cr and Ni contents of the stainless steel were suppressed with the ZnO films as the molarity increased. The compositions for Zn and O were observed to increase consistently with molarity. The coated films enhanced the corrosion potential as well as corrosion resistance of 316L SS. The corrosion potential was found to increase with molarities with 0.3 M solution of zinc acetate having the highest value of corrosion potential as compared to other coated samples.

Declaration of Competing Interest

The authors declare that they have no known competing financial interests or personal relationships that could have appeared to influence the work reported in this paper.

CRediT authorship contribution statement

Victor Adewale Owoeye: Conceptualization, Methodology, Software, Writing – original draft. **Emmanuel Ajenifuja:** Data curation, Software. **Abiodun Eyitayo Adeoye:** Visualization, Investigation. **Ayodeji Olalekan Salau:** Methodology, Writing – review & editing. **Saheed Adekunle Adewinbi:** Writing – review & editing. **Adedeji Tomide Akindadelo:** Writing – review & editing. **David A. Pelemo:** Validation. **Abimbola Patricia I. Popoola:** Validation.

References

[1] K. Baranidharan, S. Thirumalai Kumaran, M. Uthayakumar, P. Parameswaran, A review of electrochemical corrosion on stainless steel 316, Incas Bull. 12 (4) (2020) 221–226.

[2] H. Alves, D.C. Agarwal, H. Werner, Nace, International Corrosion Conference Series, (2006), Houston, 62221.
[3] A. Pardo, M.C. Merino, A.E. Coy, F. Viejo, R. Arrabal, E. Matykina, Pitting corrosion behaviour of austenitic stainless steels – combining effects of Mn and Mo additions, Corros. Sci. 50 (6) (2008) 1796–1806.
[4] H. Nezzari, R. Saidi, A. Taabouche, M. Messaoudi, M.A. Aida, Substrate temperature effect on structural and optical properties of zno thin films deposited by spray pyrolysis, J. Defect Diffus. Forum 397 (2019) 1–7.
[5] A. Ashour, M.A. Kaid, N.Z. El-Sayed, A.A. Ibrahim, Physical properties of zno thin films deposited by spray pyrolysis technique, Journal of Applied Surface Sci. 252 (2020) 7844–7848.
[6] I.Z. Abbasi, A. Khan, M. Willander, Fabrication of uv photodetector based on coral reef like p-NiO/n-ZnO nanocomposite structures, J. Mater. Lett. 108 (2013) 149.
[7] A.P. Rambu, V. Nica, M. Dobromir, Influence of Fe-doping on the optical and electrical properties of ZnO films, J. Superlattices Microstruc. 59 (2013) 87–96.
[8] Y. Wang, C. Zhou, A.M. Elquist, A. Ghods, V.G. Saravade, N. Lu, I. Ferguson, A review of earth abundant ZnO-based materials for thermoelectric and photovoltaic applications, Proceedings Volume 10533, Oxide-based Materials and Devices, SPIE OPTO, (2018), San Francisco, California.
[9] J. Song, S.A. Kulinich, J. Yan, Z. Li, J. He, C. Kan, H. Zeng, Epitaxial zno nanowire-on nanoplate structures as efficient and transferable field emitters, J. Adv. Mater 25 (40) (2013) 5750–5755.
[10] C. Pan, L. Dong, G. Zhu, S. Niu, R. Yu, Q. Yang, Y. Liu, Z.L. Wang, High-resolution electroluminescence imaging of pressure distribution using a piezoelectric nanowire led array, J. Nat. Photon 7 (2013) 752–758.
[11] H. Chen, C. Tan, D. Sun, W. Zhao, X. Tian, Y. Huang, Ultrawide range tuning of direct band gap in MgZnO monolayer via electric field effect, RSC Adv. 8 (2018) 1392–1397.
[12] A.O. Salau, A.S. Olufemi, G. I. Oluleye, V.A. Owoeye, I. Ismail, Modeling and performance analysis of dye-sensitized solar cell based on zno compact layer and tio2 photoanode, Journal of Materials Today: Proceedings, https://doi.org/ 10.1016/j.matpr.2021.05.592.
[13] V.A. Owoeye, E. Ajenifuja, E.A. Adeoye, G.A. Osinkolu, A.P.I. Popoola, Microstructural and optical properties of Ni-doped ZnO thin films prepared by chemical spray pyrolysis technique, Mater. Res. Express 6 (2019) 086455.
[14] A.V. Babalola, Effect of concentration and irradiation on the optical and structural properties of ZnO thin films deposited by spray pyrolysis techniques, J. Nucl. Inst. Methods Phys. Res. B 413 (2017) 57–61.
[15] M. Laurenti, V. Cauda, Porous zinc oxide thin films: synthesis approaches and applications, J. Coat. 8 (2018) 67.
[16] S. Muhamed, K.S. Saravana, K.V. Senthil, M.A. Uma, M. Sivakumar, R.M. Sreedevi, Enhancement of anticorrosion properties of stainless steel 304 L using nanostructured ZnO thin films, J. AIMS Mater. Sci. 5 (2018) 932–944.
[17] V.A. Owoeye, E. Ajenifuja, A.E. Adeoye, A.O. Salau, A.T. Akindadelo, D. Pelemo, A.P.I. Popoola, Microstructure and anti-corrosion properties of spray pyrolyzed Ni-doped ZnO thin films for multifunctional surface protection applications, J. Eng. Res. Express 3 (2021) 025012, doi:10.1088/2631-8695/abf65f.
[18] M. Laurenti, V. Cauda, Porous zinc oxide thin films: synthesis approaches and applications, J. Coatings 8 (2018) 67.
[19] P. Jerome, S. Jacques, H. Christoph, H. Alan, S. Laurent, The physics of plasma-enhanced chemical vapor deposition for large area coating: industrial application to flat panel displays and solar cells, IOPS J. 42 (2010) 1088–1090.
[20] S.P. Nunes, B. Fernandes, E. Fortunado, P. Vilarinho, R. Marthins, Performances presented by zinc oxide thin films deposited by spray pyrolysis, J. Thin Solid Film 337 (2001) 176–179.
[21] N. Chahmat, A. Haddad, A. Ain-Souya, R. Ganfoudi, N. Attaf, M. Salah, Effect of SN doping on the properties of ZnO thin film prepared by spray pyrolysis, J. Mod. Phy., 1 (2012) 1781–2178.
[22] C.Y. Jiang, X.W. Sun, G.Q. Lo, D.L. Kwong, J.X. Wang, Improved dye-sensitized solar cells with a ZnO nanoflower photoanode, J. Appl. Phys. Lett. 90 (2007) 263501.
[23] P. Kandasamy, A. Lourdusamy, Studies on zinc oxide thin film by chemical spray pyrolysis technologies, Intern. J. Phy. Sci. 9 (2014) 261–266.
[24] S. Aydogu, O. Sendil, M.B. Coban, The optical and structural properties of zno thin films deposited by the spray pyrolysis techniques, Chin. J. Phys. 50 (2012) 112–119.
[25] M.G. Hosseini, R. Bagheri, R. Najjar, Electropolymerization of polypyrrole and polypyrrole-zno nanocomposites on mild steel and its corrosion protection performance, J. Appl. Polym. Sci. 121 (2011) 3159–3166.
[26] M. Ibrahim, K. Kannan, H. Parangusan, S. Eldeib, O. Shehata, M. Ismail, R. Zarandah, K. Sadasivuni, Enhanced corrosion protection of Epoxy/ZnO-NiO nanocomposite coatings on steel Coatings 10 (2020) 783.
[27] R. Matero, M. Ritala, M. Leskelä, T. Salo, J. Aromaa, Atomic layer deposited thin films for corrosion protection, J. de Physique IV (Proceedings) 8 (1999) 494–499.
[28] M.A. Fusco, C.J. Oldham, G.N. Parsons, Layer deposited Al2O3/TiO2 nanolaminate thin films on copper in 0.1MNaCl, J. Mater. 12 (2019) 672.
[29] A. Mohamed, P.L. Neto, L.A. Avaca, M.A. Aegerte, Sol-gel thin films for corrosion protection, J. Ceram. Intern. (1995) 403–406.
[30] J. Cambon, F. Ansart, J. Bonino, V. Turq, Effect of cerium concentration on corrosion resistance and polymerization of hybrid sol-gel coating on martensitic stainless steel, Prog. Org. Coat. 75 (2012) 486–493.
[31] Z. Ahmad, A.B. Jabbar, K. Abdullahi, M. Abbas, Effect of scandium doping on the corrosion resistance and mechanical behavior of al-3mg alloy in neutral chloride solutions, Materials Sciences and Applications 2 (2011) 244–250.
[32] D.M. Martinez de la Escalera, J.J. Ramos-Hernandez, E. Porcayo-Palafox, J. Porcayo-Calderon, J.G. Gonzalez-Rodriguez, and L. Martinez-Gomez, Effect of Nd3+ ion concentration on the corrosion resistance of API X70 steel in chloride-rich environments, Advances in Materials Science and Engineering, Volume 2018 Article ID 9328317. https://doi.org/ 10.1155/2018/9328317.
[33] V.A. Owoeye, E. Ajenifuja, B. Babatope, G.A. Osinkolu, A. P. I. popoola and 0. popoola, experimental investigation and numerical simulation of mechanical properties and thermal stability of tin alloy processed by equal channel angular extrusion (ECAE), J. Eng. Res. Exp. 1 (2019) 025030.
[34] M.A. Eleruja, G.O. Egharevba, A.O. Abulude, O.O. Akinwunmi, C. Jeynes, E.O.B. Ajayi, Preparation and characterization of metalorganic chemical vapor deposited nickel oxide and lithium nickel oxide thin films, J. Mater. Sci. 42 (2007) 2758–2765.
[35] S.A. Adewinbi, W. Buremoh, V.A. Owoeye, Y.A. Ajayeoba, A.O. Salau, H.K. Busari, M.A. Tijani, B.A. Taleatu, Preparation and characterization of tio2 thin film electrode for optoelectronic and energy storage potentials: effects of Co incorporation, Chem. Phys. Lett. 779 (2021) 138854, doi:10.1016/j.cplett.2021.138854.
[36] R. Swapna, M. Ashok, G. Muralidharan, M.C. Santhosh Kumar, Microstructural, electrical and optical properties of ZnO:MO thin films with various thickness by spray pyrolysis, J. Anal. Appl. Pyrolysis 102 (2013) 68–75.
[37] S. Suzuki, T. Miyata, M. Ishii, T. Minami, Transparent conducting V-co-doped AZO thin films prepared by magnetron sputtering, Thin Solid Films 434 (2003) 14–19.
[38] R. Amari, A. Mahroug, A. Boukhari, B. Deghfel, N. Selmi, Structural, optical and luminescence properties of zno thin films prepared by sol-gel spin–coating method: effect of precursor concentration, Chin. Phys. Lett 35 (1) (2018) 016801–016813.
[39] M.N. Amroun, M. Khadraoui, Effect of substrate temperature on the properties of SnS2 thin films, Optik (Stuttg) (2019), doi:10.1016/j.ijleo.2019.03.011.
[40] G. Ojeda-Barrero, A.I. Oliva-Avilés, A.I. Oliva, R.D. Maldonado, M. Acosta, G.M. Alonzo-Medina, Effect of the substrate temperature on the physical properties of sprayed-CdS films by using an automatized perfume atomizer, Mater. Sci. Semicond. Process. 79 (2018) 7–13.
[41] A.M. AL-Diabata, N.M. Ahmed, M.R. Hashim, K.M. Chahrour, M. Bououdina, Effect of deposition temperature on structural and optical properties of chemically sprayed ZnS thin films, Procedia. Chem. 19 (2016) 485–491.
[42] E. Karakose, H. Çolak, Effect of substrate temperature on the structural properties of ZnO nanorods, Energy 141 (2017) 50–55.
[43] L. Tang, A study of the polarization techniques for corrosion rate measurement in a steel concrete system, 9DBMC 158 (2002) 1–10.
[44] L.E. Greene, General route to vertical ZnO nanowire arrays using textured ZnO seeds, J. Nano Lett. 5 (2005) 1231–1236.

[45] G. Singla, K. Singh, O. Pandey, Williamson, Hall study on synthesized nanocrystalline tungsten carbide (WC), J. Appl. Phys. 113 (2013) 237–242.
[46] E. Ajenifuja, G.A. Osinkolu, A.Y. Fasasi, D.A. Pelemo, E.I. Obiajunwa, Rutherford backscattering spectroscopy and structural analysis of DC reactive magnetron sputtered titanium nitride thin films on glass substrates, J. Mater. Sci. 27 (2016) 335.
[47] O.O. Akinwunmi, J.A.O. Ogundeji, A.T. Famojuro, O.A. Akinwumi, O.O. Ilori, O.G. Falodun, E.O.B. Ajayi, Preparation of some properties of metal organic chemical vapour deposited Al-doped ZnO thin films using single solid precursor, J. Mod. Phy. 9 (2018) 2073–2089.
[48] G. Kaur, A. Mitra, K.L. Yadav, Progress in natural science, J. Mater. Internat. 25 (2015) 12–21.
[49] O. Bayram, E. Sener, E. İgman, O. Simsek, Investigation of structural, morphological and optical properties of Nickel-doped Zinc Oxide thin films fabricated by co-sputtering, J. Mater. Sci. Mater. Electron. 30 (2019) 3452–3458.
[50] B.A. Taleatu, E.A. Arbab, G.T. Mola, Mater. Sci. Semicond. Process. 44 (2016) 85.
[51] B. Taleatu, L. Cozzarini, B. Olofinjana, G. Bertolini, S. Adewinbi, S. Behrendt, Mater. Sci. Semicond. Process. 87 (2018) 155.
[52] S.A. Adewinbi, R.A. Busari, O.E. Adewumi, B.A. Taleatu, Effective photoabsorption of two-way spin-coated metal oxides interfacial layers: surface microstructural and optical studies, Surf. Interfaces 23 (2021).
[53] Y.Y. Chen, T. Duval, U.D. Hung, J.W. Yeh, H.C. Shih, Microstructure, and electrochemical properties of high entropy alloys—A comparison with type-304 stainless steel, J. Corros. Sci. 47 (2005) 2257–2279.
[54] M.S. Kaiser, S.H. Sabbir, M. Rahman, M.S. Kabir, M. Al Nur, Effect of Fe, Ni and Cr on the corrosion behaviour of hypereutectic Al-Si automotive alloy in 3.5% NaCl solution at different temperature and velocity, J. Mechan. Eng. 48 (2018) 11–17.
[55] A. Clarke, Temperature and the metabolic theory of ecology, J. Funct. Ecol. 20 (2006) 405–412.
[56] M.S. Kaiser, Effects of solution treatment on wear behaviour of Al-12Si-1mg piston alloy containing trace Zr, mayfeb, J. Mater. Sci. 1 (2016) 27–38.